6.0 DEVELOPMENT OF A REMOTE-fNIRS DEVICE

Dr. Leanne Hirshfield (Outerfacing Technology)

6.1 Introduction

Recent advancements in biotechnology have resulted in brain measurement devices that can non-invasively measure the functioning brain in people's natural environments. Functional Near-Infrared Spectroscopy (fNIRS) is such a technique, which measures the hemoglobin signatures related to neural activation. With the potential to monitor people's mental states non-invasively and in real-time, researchers have used fNIRS devices to measure a myriad of cognitive and emotional states in operational settings [1-4]. Leading biotechnologists have created wireless implementations (Fig 1) of fNIRS for real-time brain monitoring under normal working conditions [4]. The device works by pulsing near-infrared light into the head, and using powerful light detectors to measure the light that is reflected back out of the head. The fNIRS is unique in its potential to take these measurements from a distance, without requiring contact with the head. While fNIRS implementations for measuring brain function have used source and detection fibers which are placed on the head of subjects directly, we have demonstrated that it is possible to modify this technology so that measurement of brain function can be done at a distance from the user.

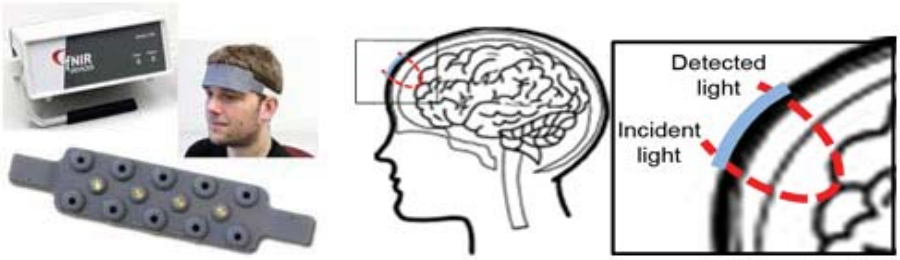

Figure 4-1. Left: an example of wireless fNIRS currently available from Biopac. Right: Near-infrared light is pulsed into the brain cortex. Reflected light is determined with optical detectors.

Specifically, with research support from this effort[2], we have developed a remote-fNIRS system (placed 0.6 meters from participants) to demonstrate the feasibility of taking fNIRS measurements from a distance and we have run a series of experiments to validate the device.

The capability to measure brain activation from a distance would be valuable in a number of applications, including, but not limited to the following:

1) Monitoring of personnel could be done to measure the neural correlates related to a range of mental states such as cognitive load, trust, suspicion, complacency, and frustration.
2) Monitoring of sensitive populations (patients with mental illness, TBI, or PTSD, etc.) in a manner that would eliminate the discomfort of wearing constricting sensors on the head. Mobile, hand-held remote-fNIRS devices could be developed to take these measurements in a range of operational settings.
3) Helmets, hats, and augmented reality displays (like Google Glass) could be embedded with a camera and light source add-on that would enable unobtrusive continuous brain measurement without requiring sensor contact with the head.

[2] This research took place over the course of several years, and it would not have been possible without support from a team of exceptional researchers, as listed in the acknowledgements section.

4) Scanners at high security entry control points (ECP's) such as airports could be equipped with remote-fNIRS sensors to search for neural correlates of deception, anxiety, or other signs of malintent from people passing through.

The rest of this report proceeds as follows. We first provide a description of the principles underlying traditional head-mounted fNIRS. Then we describe the current remote-fNIRS set-up and the validation experiments conducted thus far to demonstrate feasibility. At the end we point readers to all code and user manuals that were created over the course of this project. Lastly, we acknowledge all of the team members that played a role at various points throughout the project.

6.2 Functional Near-Infrared Spectroscopy

The basis of fNIRS is the usage of near-infrared light, which can penetrate the scalp and skull to reach the brain cortex. Optical fibers are placed on the surface of the head for illumination and detection fibers are placed on the head to measure light which reflects back. Due to the scattering nature of tissue, light which is measured at a distance from the illumination point has travelled deeper into tissue (Fig 2). Typically, detection fibers are placed ~3cm away from the source fiber to guarantee that light has interacted with brain tissue. Since two wavelengths of light are typically used in the near-infrared wavelength range (650-850 nm), spectral features of hemoglobin can be measured. Particularly, concentration changes in oxy- and deoxy-hemoglobin can be distinguished. Due to neuro-vascular coupling, changes in hemoglobin concentration can be used for measuring the vascular effect of brain activation [5-6].

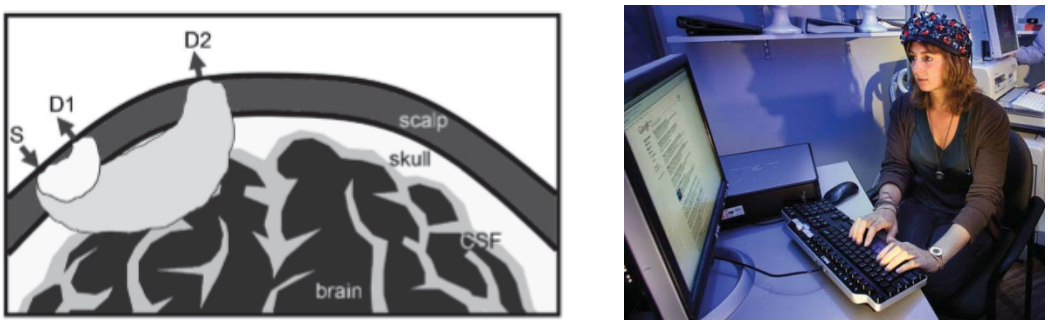

Figure 4-2. Left-Schematic showing the differences in penetration depths between the two source-detector separation distances [9].

6.3 Remote-fNIRS System and Validation Experiments

During this project, we developed, and tested the accuracy of, a remote-fNIRS system with support from AFRL-RHXS. The remote-fNIRS system is depicted in Figure 3, and we describe the details of the system in this section.

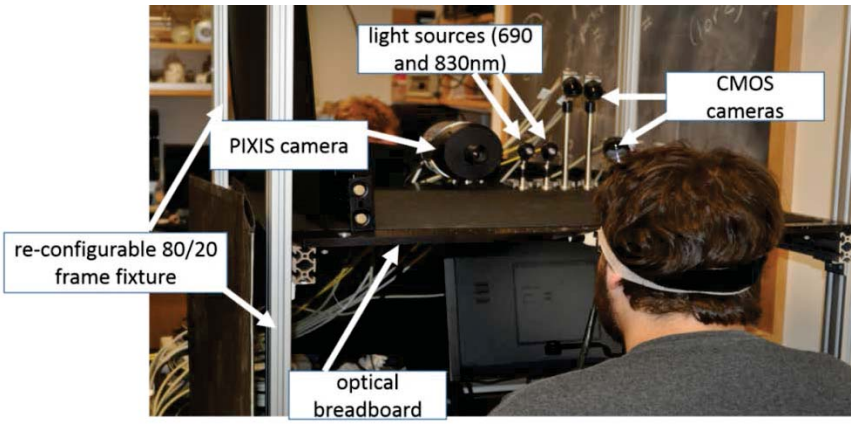

Figure 4-3. The remote-fNIRS system setup is designed to be easily configured for transportation, and for being used in a variety of experimental settings.

In the creation of the remote-fNIRS system, it was necessary to characterize the ability to measure changes in sampled light intensities over time with a high level of confidence. To ensure that the decreased intensity of light over a distance was measureable, a sensor that is sensitive to the wavelengths of interest was needed (650-850 nm). Traditional consumer grade CCD sensors have peak quantum efficiency (QE) of ~30%, while many contact fNIRS devices use either electron multiplier tubes or photomultiplier tubes to increase quantum efficiency to much higher values. We identified a CCD technology that increases the QE in the NIR bands to ~70% by sampling light from the backside of a thickened CCD sensor, referred to as deep-depletion. The Princeton Instruments PIXIS 512B imager (Fig. 2) is a cooled-deep depletion CCD with a mechanical shutter and 16-bit analog to digital converter. The mechanical shutter ensures that light from the previous frame does not 'bleed into' subsequent frames.

The ThorLabs MCLS-1 Multiple Channel Laser supplies the light sources for this project. Two wavelengths were chosen, 690nm and 830nm, since those wavelengths are typically used for hemoglobin measurements in the brain. Furthermore, the light source accepts a hardware modulation signal or serial commands through USB, which allows us to either modulate the light sources at a given frequency or multiplex the two sources. The operation of the source can be manipulated through this hardware modulation line to turn on/off each of the sources, alternately. Using the same pulse source, the PIXIS device can be triggered to collect an image, ensuring that the image contains the wavelength of interest.

We then built a configurable experimentation station that contains an optical breadboard from Thorlabs. This makes it possible to easily move the cameras, camera angles, height of cameras, etc., depending on the experiment we want to run, and the areas on participants that we are interested in measuring. We designed the software and hardware configurations using LabView to enable a working remote-fNIRS that pulses the light sources (690nm and 830nm) and takes pictures at the correct syncing rate to collect measurements of these light sources as they are reflected out of a material (such as phantom material, or an arm or head).

6.3.1. Capability to Measure Many Locations with Images

One important advantage that remote-fNIRS has over traditional head-mounted fNIRS is our capability to create many 'light detectors', resulting in many areas of the brain measured. Traditional fNIRS devices measure one brain location via one source-detector pairing (Fig 2). Expensive photomultiplier tubes are used for the light detectors, making fNIRS devices increase dramatically in price as the number of detectors are increased. As described next, the remote-fNIRS does not share this constraint.Our software finds the center of the light source in the

images and extracts the reflected light intensities (690nm and 830nm) at a pixel location measured to be 3cm from the center of the light source in the image (Figure 4).

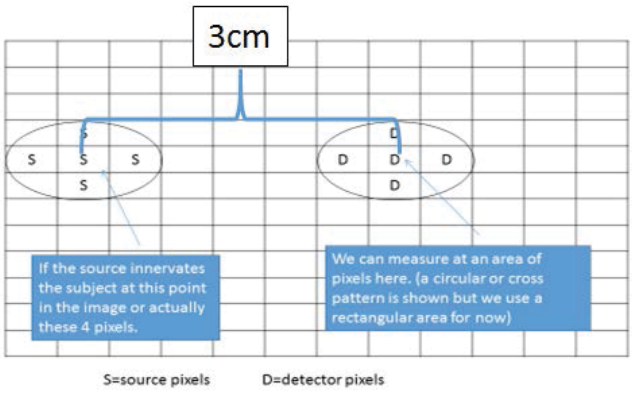

Figure 4-4. Our algorithms take an image from the camera and automatically find the center of the light insertion point (source). We then choose specific distances from the source insertion point to extract light intensity, and essentially create our own 'light detector.'

By looking at different distances from the source insertion point, we can create multiple detectors, resulting in multiple source-detector pairings. Each source-detector pairing results in a new channel of data, enabling us to measure another area of the brain (Figure 5).

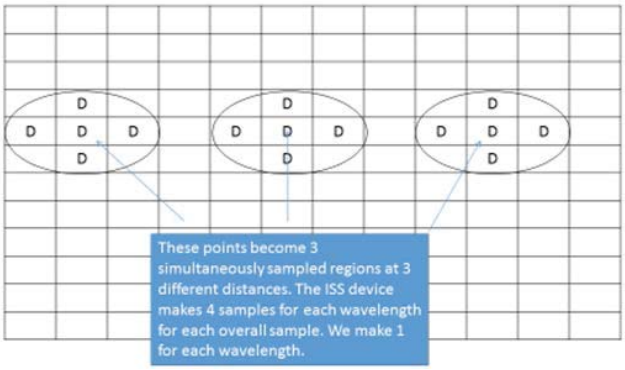

Figure 4-5. By looking at different distances from the source insertion point, we can create multiple detectors, resulting in multiple source-detector pairings. Each source-source detector pairing resulting in a new channel of data, enabling us to measure another area of the brain.

By extracting light intensity values from different pixels in the image, we can create many 'detectors' all around a light source insertion point. Unlike traditional head mounted fNIRS systems that include the cost of new photomultiplier tubes for each new detector, we can readily add detectors by extracting light from different regions of the image. This approach allows us to collect channels of data in a 3.5 cm radius surrounding the source insertion point.

6.4 Round 1 Validation Experiments

Three experiments were conducted to validate the remote-fNIRS device by comparing its measurements to simultaneous measurements taken with the ISS Oxiplex, a commercial fNIRS

device. The ISS OxiplexTS is a frequency-domain tissue spectrometer (Figure 6). The ISS device comes with two probes. Each probe has a detector and four light sources. Each light source produces near-infrared light at two wavelengths (690nm and 830nm) which are pulsed intermittently in time. In our validation studies, we compare the data from the remote-fNIRS to the data acquired by the ISS device. All three validation studies involve simultaneous measurements with the on-body ISS fNIRS and the remote-fNIRS. The three studies included:

1) Systemic Blood Flow Changes in the Arm (n = 10): As a first step, we took simultaneous measurements with the remote-fNIRS and the commercial ISS device on participants' arms while the blood flow to the arm was occluded for 3 minutes, resulting in a decrease in oxy-hemoglobin.
2) Systemic Blood Flow Changes in the Brain (n = 8): Next, we took simultaneous measurements with the remote-fNIRS and the commercial ISS device on participants' foreheads while they held their breath for 20 seconds at a time, repeating the process several times.
3) Functional Blood Flow Changes in the Brain (n = 10): Next, we took simultaneous measurements with the remote-fNIRS and the commercial ISS device on participants' foreheads while they completed a simple verbal working memory task.

Figure 4-6. On the ISS device, the light sources and detectors embedded into two rubber probes. A detector and set of light sources (s1, s2, s3, and s4) are placed on the head.

6.4.1. Arm Occlusion Experiment

For our first study, we used an arterial arm occlusion experiment because it is known to produce large changes in hemoglobin concentration, as measured by fNIRS.

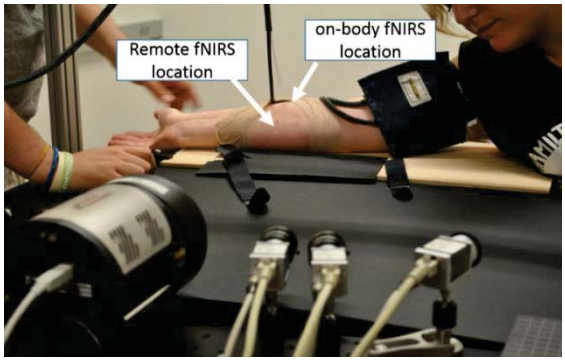

Figure 4-7. Arm occlusion study set-up.

Simultaneous measurements with the on-body (ISS) and the remote-fNIRS sensors were taken. In order to avoid interference between the light sources and detectors, the ISS probe was placed on the other side of the arm as seen in Figure 7. Ten individuals participated in the experiment, with each individual partaking in two trials of the experiment. Measurements were taken for one minute of baseline, then arm occlusion using a sphygmomanometer at 180mmHg occurred for three minutes, with a final two minutes of rest occurring to allow the blood flow in participants' arms to return to baseline. This resulted in a total of 360 seconds (6 minutes) per arm trial. After several minutes of rest, measurements were repeated with the positions of the ISS device and the remote device switched, resulting in 20 occlusions total (10 subjects, repeated twice).

The ISS device was set to sample at 2 Hz and the PIXIS camera sampled at 2.13 Hz throughout the experiment. Since large source-detector distances are needed for sampling the brain, we chose to analyze only the data resulting from the 3 cm source-detector distance, not the shorter distances. For the remote NIRS data only those pixels of the camera were analyzed, which also correspond to 3 cm source-detector distance.

Preprocessing of the data included detrending and normalizing light intensity values in each channel by their own baseline values. We then applied a moving average band pass (.5 and .01 Hz) filter to the data and we used the modified Beer-Lambert Law [8, 19] to convert our light intensity data to measures of the change in oxygenated hemoglobin (ΔO) and deoxygenated hemoglobin (ΔD) in the brain.

The top of Figure 8 shows the group average of oxygenated (ΔO) and deoxygenated (ΔD) hemoglobin concentration changes, as well as the corresponding error bars, across all 10 participants for trials 1 and 2 as measured by the ISS device. The bottom of the figure shows the ΔO and ΔD as measured by the PIXIS camera. For the PIXIS data four data sets have been discarded due to motion artifacts.

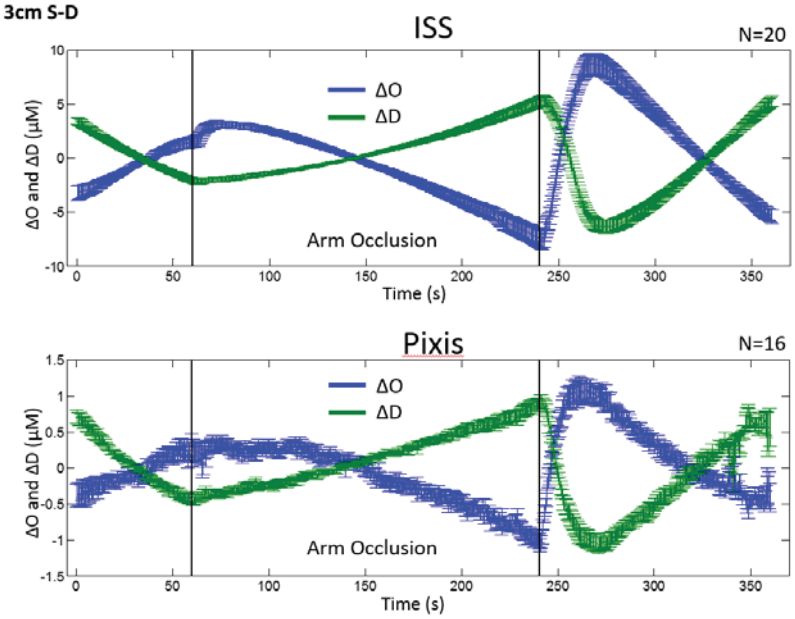

Figure 4-8. The average ΔO and ΔD, as well as the corresponding error bars, across all 10 participants for trial 1 and trial 2 (resulting in total n of 20) as measured by the ISS device (top) and remote PIXIS camera (bottom). The two vertical black lines in each figure represent the times that occlusion began and ended.

Visually, it is clear from the graphs that both the ISS device and the PIXIS device were able to measure the effect of arterial occlusion on oxygenated and deoxygenated hemoglobin. It is promising to note that the PIXIS camera was sensitive to both wavelengths of 690 and 830nm at a source detector distance of 3 cm, which is needed to generate values of ΔO and ΔD changes in the brain. Also, it is promising to see the similarities between the ISS data and that acquired by the remote PIXIS set-up. Having said that, the PIXIS data does have a lower signal-to-noise ratio (SNR) as indicated by the larger error bars and smaller signals.

6.4.2. Brain imaging – a Breath Holding Experiment

Next, we conducted an experiment to measure systematic changes in the brain caused by breath holding. Measurements were taken for 1 minute of baseline, and participants sat with their eyes closed and their heads held by a chin rest to reduce motion. Then participants were instructed to hold their breath after exhalation for 20 seconds at a time, followed by 40 seconds of rest. They repeated this process (20 seconds of breath holding and 40 seconds to recover) for 3 minutes total. Finally, participants rested for 1 minute while the blood flow in their head returned to baseline. Thus, each experiment lasted for 5 minutes.

The same process as that described in section 5.1 was used on this experiment data. Figure 9 shows the average ΔO and ΔD, as well as the corresponding error bars, across 7 participants as measured by the ISS device (top) and remote PIXIS camera (bottom). Data from 1 subject was excluded due to motion. The vertical black lines in each figure represent the times of breath holding (BH).

Once again, results are promising as we see similar activation with the ISS and remote-fNIRS devices (although the remote-fNIRS again has more noise in the signal and a lower magnitude).

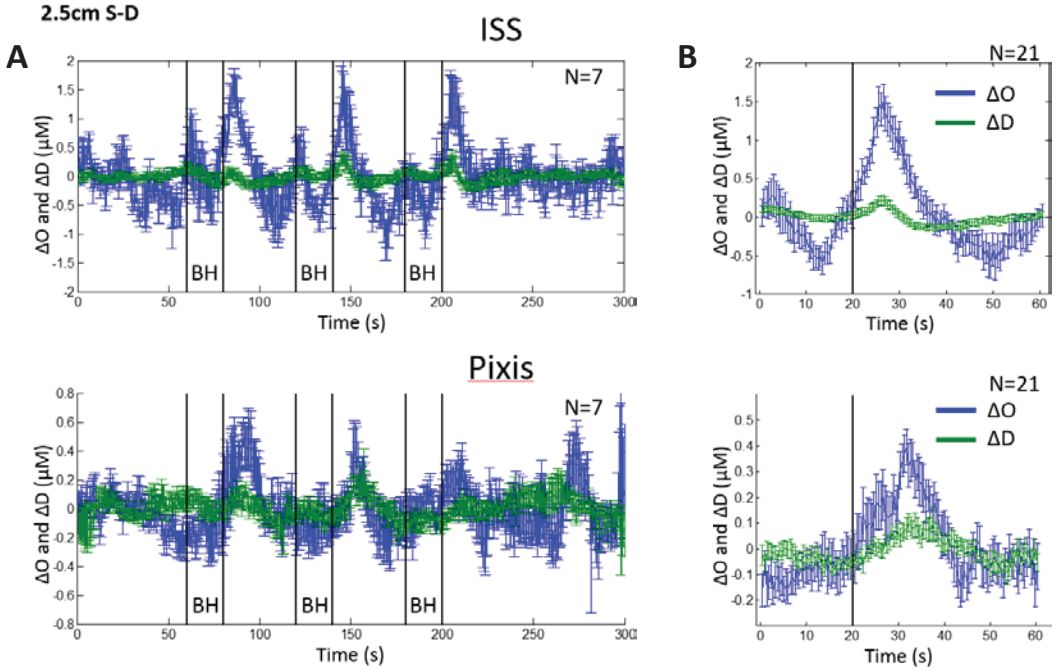

Figure 4-9. The average ΔO and ΔD, as well as the corresponding error bars, across 7 participants as measured by the ISS device (top) and remote PIXIS camera (bottom) over time. The vertical black lines represent breath holding (BH). B) Same data set, but further averaged over the three breath holding periods.

6.4.3. Functional Brain Imaging—A Workload Experiment

The arm occlusion and breath holding experiments involved well validated techniques for limiting the blood flow and/or oxygenation of the blood in the arm and head regions. These techniques have been repeatedly found to cause systemic changes in people's bodies, and we demonstrated our capability to measure those changes remotely.

The next step involves the measurement of functional brain activation—where the brain is activated in specific brain regions while a person conducts an information processing task. Much of our prior research has used commercial fNIRS devices to measure, and predict, mental states such as workload, frustration, trust, and suspicion by looking at the blood flow in specific brain regions [12-14]. A remote-fNIRS capable of making these predictions would be valuable in the human performance domain. Thus, our final experiment was based on a well validated working memory task, called the n-back task. While sitting with their heads in a chin rest to reduce motion, participants did the 1back and 3back version of the nback experiment, with 15 seconds of rest inserted after each task to allow the brain to return to baseline. The 3back task requires participants to hold, and manipulate, three items in working memory at a time, while the easier 1back task only requires one item at a time to be held in working memory.

Measuring functional brain activation, such as that caused by an nback task, is more difficult than measuring the systemic changes of breath holding and occlusion because localized regions of activation could be missed with a small number of sensors, and individual differences in brain activation can make it difficult to find average trends across participants. With this in mind, we ran two sessions of the experiment for each participant. In the first session they completed the nback tasks with the ISS fNIRS placed on the right side of the forehead and the remote-fNIRS focused on the left side of the forehead. In the second session we switched the locations, so that the ISS and remote-fNIRS each had an opportunity to take nback measurements from the left and right sides of the forehead.

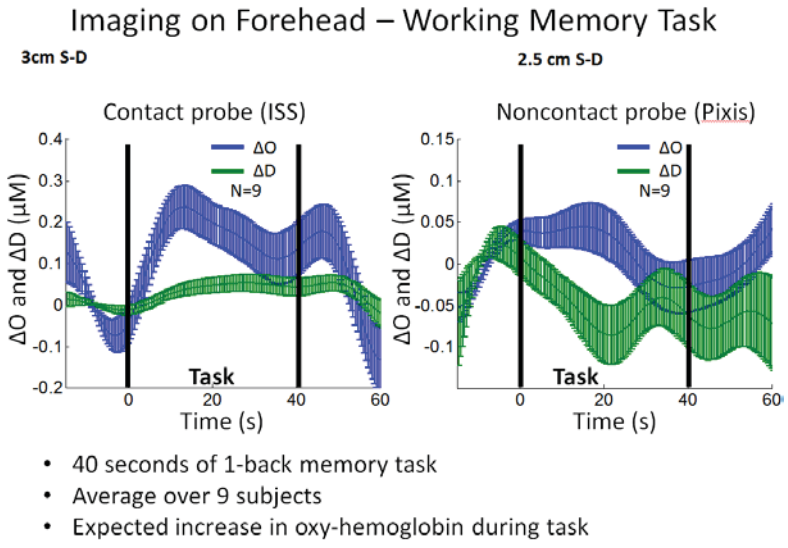

Figure 4-10. The average ΔO and ΔD, as well as the corresponding error bars, across 9 participants as measured by the ISS device (left) and remote PIXIS camera (right) over time.

The results (averaged across both hemispheres and all participants) from the nback experiments are available in Figure 10. Although we see the expected trend of oxy-hemoglobin increasing and then leveling off during the tasks, the results were not as nicely synchronized as with the

occlusion and breath holding studies. We identified several experimental design issues that may have affected the data, and we just completed data collection (n = 12) on another workload experiment. In particular, we changed our task to the multitasking scenario in the Multi-Attribute Task Battery, and we only measure one location in the center of the forehead (the FpZ site) to remove the effects of individual differences with regard to brain lateralization on the data[3].

It is also likely that small participant movements caused by participants' use of the mouse and keyboard—despite their chins being placed in a chinrest-- may have caused motion artifacts in signal, further confounding the results.

6.5 Round 2 Validation Experiments: Including CMOS Cameras and Motion Artifact Correction

We also created a more cost-efficient version of the remote fNIRS that includes two CMOS cameras (Figure 11), where each camera is configured to measure a different light intensity, in the example provided, either the 690nm or the 830nm light intensities, enabling the wavelengths of light to be multiplexed rather than modulated. These imagers are much lower cost and have a smaller footprint than the relatively large and cumbersome PIXIS camera. Each imager with lens is ~4x2x2 inches, while the PIXIS is >8x4x4 inches.

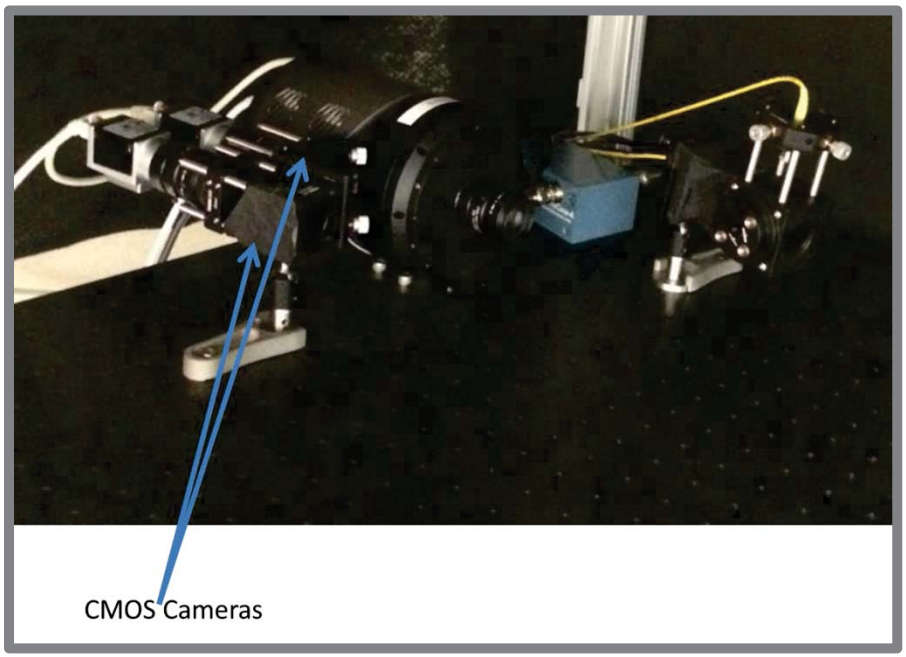

Figure 4-11. CMOS cameras added to experimental set-up

After setting up the CMOS cameras, another round of validation studies was run to establish the feasibility of the CMOS and PIXIS based remote fNIRS systems. We also noticed during our first round of experiments that even though participant movement was minimized, very small movements did create motion artifacts in the resulting data. Therefore, we researched a myriad of motion correction signal processing techniques (see Appendix) into our data analysis, and we modified our data processing code to incorporate motion artifact correction on the data, as reflected in the results below.

[3] Data is currently being analyzed. Initial results available upon request to Dr. Hirshfield.

6.5.1. Experiment 1: Leg Occlusion

For the leg occlusion study, 11 participants were recruited and written consent was obtained from all subjects after a description of the study. The commercial fNIRS probe was attached 55% of the way from the ankle to the knee on the inner right calf. The laser of the remote fNIRS (comprised of a 685 nm and 830 nm laser and either a PIXIS or two CMOS cameras) was trained on the same spot on the other side of the same calf. Participants were seated with their right leg extended on a small stool, instructed not to move, and the leg was secured using velcro straps. After 60 s of rest, a blood pressure cuff attached just above the knee was inflated to 160 mmHg for 180 s. After deflation, there was a 120 s period of rest. Upon completion, subjects were instructed to stand up and move around to return to a normal state of blood flow before the trial was repeated using the other type of camera. The order of the cameras was pseudo-randomized.

A blob detection algorithm was used to automatically detect the light source insertion point in all images and then to automatically extract light intensity values (685nm and 830nm) at 3cm distance from the source insertion point for all CMOS and PIXIS images. This results in a dataset of raw light intensity data at a 3cm source-detector distance for the CMOS based remote fNIRS, and another dataset for the PIXIS based remote fNIRS. This is the same format as the raw data output of the ISS device. Thus, from this point on, all data is filtered and pre-processed in the same exact way, to ensure fair comparisons.

All data is bandpass filtered between .01 and .5 Hz, and a sliding window averaging technique is used to smooth the resulting data. Then the MARA motion artifact correction algorithm, which does spline interpolation based on a sliding standard deviation of the data, is applied to the dataset. Next, the modified beer-lambert law is used to convert the raw light intensity values into relative changes in oxy and deoxy-hemoglobin, as shown in the resulting graphs. The graphs in Figure 12 show the data averaged across all participants in the experiment with standard error bars included.

PIXIS	CMOS	ISS
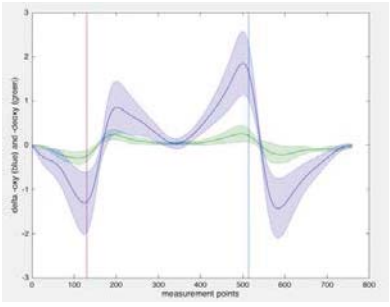	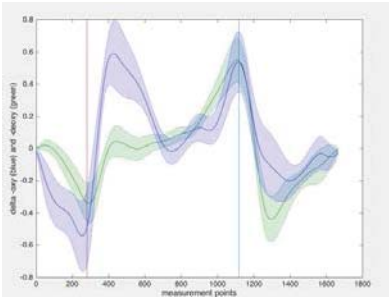	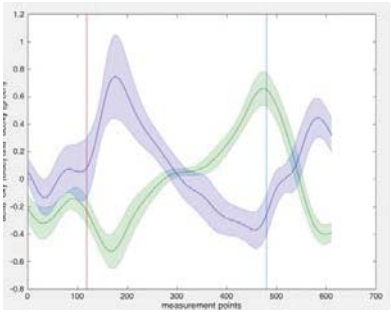

Figure 4-12. Results from Leg Occlusion Study

6.5.2. Experiment 2: Breath Holding

For the breath holding study, 12 participants were recruited and written consent was obtained from all subjects after a description of the study. The commercial fNIRS was attached with the right edge of the probe 1 cm to the left of the center of the forehead, ensuring that the probe's light detector was on the far side to limit interference from the remote fNIRS. The laser of the remote fNIRS (comprised of a 685 nm and 830 nm laser and either a PIXIS or two CMOS cameras) was focused 3 cm above the right eyebrow and 3 cm to the right of the center of the subject's forehead. Participants were trained to exhale all of their breath quickly and hold it when

instructed. Subjects' heads were then secured to a chinrest using spandex material, with their forehead against a metal frame. Data was collected as participants breathed normally for 60 s then held their breath for 30 s with a 90 s rest that followed. Participants then repeated the 30 s breath hold and 90 s rest. Upon completion, the trial was repeated using the other type of camera. The order of the cameras was pseudo-randomized.

A blob detection algorithm was used to automatically detect the light source insertion point in all images and then to automatically extract light intensity values (685nm and 830nm) at 3cm distance from the source insertion point for all CMOS and PIXIS images. This results in a dataset of raw light intensity data at a 3cm source-detector distance for the CMOS based remote fNIRS, and another dataset for the PIXIS based remote fNIRS. This is the same format as the raw data output of the ISS device. Thus, from this point on, all data is filtered and pre-processed in the same exact way, to ensure fair comparisons.

All data is bandpass filtered between .01 and .5 Hz, and a sliding window averaging technique is used to smooth the resulting data. Then the MARA motion artifact correction algorithm, which does spline interpolation based on a sliding standard deviation of the data, is applied to the dataset. Next, the modified beer-lambert law is used to convert the raw light intensity values into relative changes in oxy and deoxy-hemoglobin, as shown in the resulting graphs. The graphs in Figure 13 show the data averaged across all participants in the experiment with standard error bars included.

PIXIS	CMOS	ISS
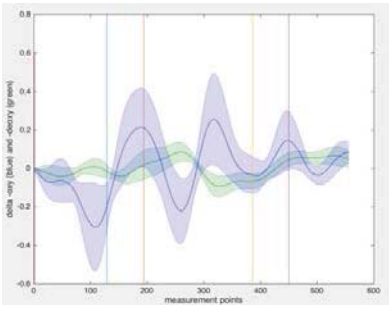	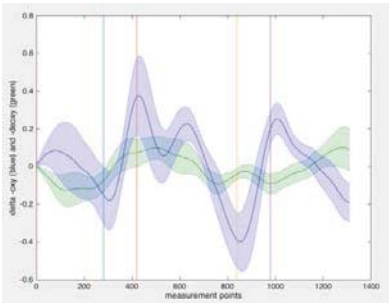	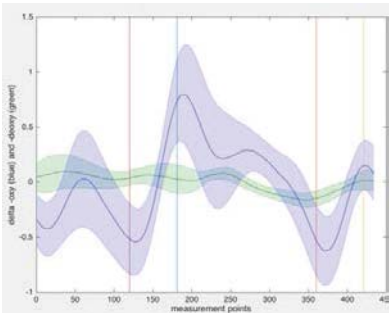

Figure 4-13. Results from Breath Holding Study

6.5.3. Experiment 3: MATB versus Controlled Rest Workload Study

Issues with our first (round 1 validation studies) workload study from last summer stemmed from the task chosen and the probe placements. In the first workload study, the n-back task was not difficult enough to create consistent functional activation in the regions that our sensors were placed. Therefore, we chose to use the Air Force Multi-Attribute Task Battery (MATB) as our task, as the multi-tasking scenario creates much more functional brain activation than the n-back task. Also, we are limited by the number of measurement channels available with each fNIRS device. In the first workload study, we chose to measure one region on the left and one region on the right side of the brain during studies. We believe that individual differences in the lateralization between the two hemispheres of the brain made it difficult for us to interpret our results when we averaged the data across participants. Therefore, in this study we only made measurements in the center of the forehead, at the FpZ location on the forehead, in order to avoid these lateralization issues.

Twelve participants were gathered for the workload study and written consent was collected after a description of the study. Participants were trained on the AF_MATB program the week prior to data collection. They were instructed on the objectives and controls of the program before playing 5 min of the easy difficulty setting and then completed a NASA TLX survey. This was repeated for the moderate and high difficulty settings. Upon arrival for data collection, participants were re-trained for 90 s on the high difficulty setting and completed a TLX survey. Their performance, survey responses, and a short qualitative interview were used to determine the difficulty that would be used for their trials (either moderate or difficult). Subjects who ranked their frustration higher than 10 on the TLX or expressed uncertainty on their performance in the interview were assigned the moderate setting. Participants' heads were secured to an upright chinrest using spandex material while their head rested against a metal frame. Three trials were conducted each with the commercial fNIRS, the CMOS cameras or the PIXIS camera. In each trial the sensor was focused just to left of the FpZ location while the light source(s) was just to the right. Participants had two tasks during the trials. The first was to look at a MATB screenshot with the word "REST" across the center; this was the control (Figure 14). The second was to actually play the MATB program at their appropriate difficulty setting. The trial began with 60 s control, followed by 4 cycles of 90 s gameplay then 60 s control. The order of the sensors was pseudo-randomized.

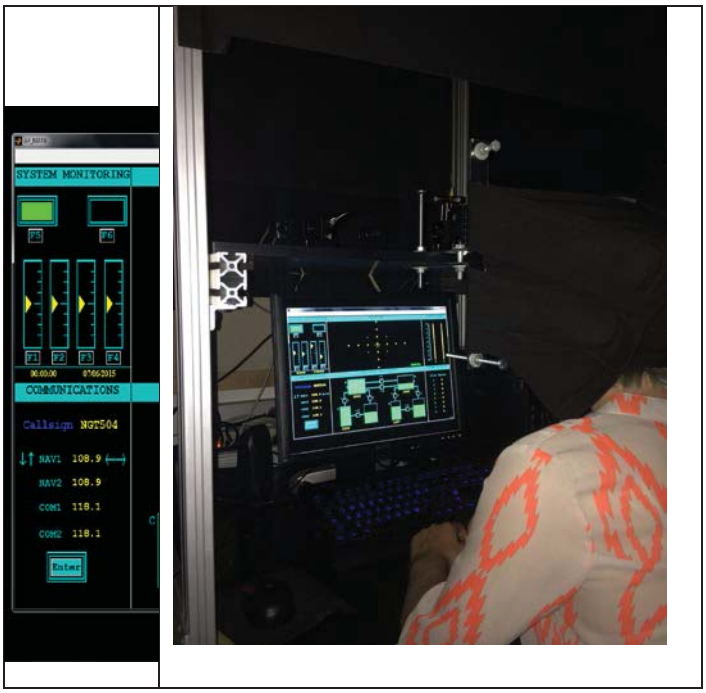

Figure 4-14. MATB Experimental Set-Up

A blob detection algorithm was used to automatically detect the light source insertion point in all images and then to automatically extract light intensity values (685nm and 830nm) at 3cm distance from the source insertion point for all CMOS and PIXIS images. This results in a dataset of raw light intensity data at a 3cm source-detector distance for the CMOS based remote fNIRS, and another dataset for the PIXIS based remote fNIRS. This is the same format as the raw data output of the ISS device. Thus, from this point on, all data is filtered and pre-processed in the same exact way, to ensure fair comparisons.

All data is bandpass filtered between .01 and .5 Hz, and a sliding window averaging technique is used to smooth the resulting data. Then the MARA motion artifact correction algorithm, which

does spline interpolation based on a sliding standard deviation of the data, is applied to the dataset. Next, the modified beer-lambert law is used to convert the raw light intensity values into relative changes in oxy and deoxy-hemoglobin, as shown in the resulting graphs. The graphs in Figure 15 show the data averaged across all participants in the experiment with standard error bars included.

PIXIS	CMOS	ISS
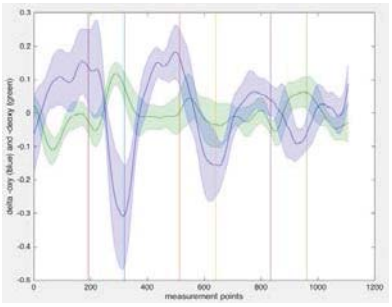	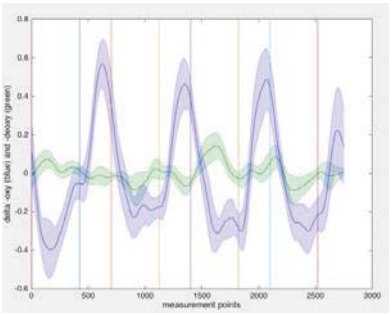	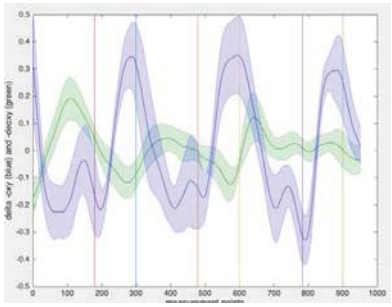

Figure 4-15. Results from MATB Experiment

6.6 Code and User Manuals

All code developed during this research is available on github so that SRA and AFRL can readily access and interpret the code. All manuals are included with this report submission.

6.7 Acknowledgements

This work occurred over the course of several years, and it would not have been possible without support, at various times, from a handful of skilled interdisciplinary researchers. This includes Mark Costa, Sergio Fantini, Sam Hincks, Rob Jacob, Jana Kainerstorfer, Chris Meier, Lanie Monforton, Ben Parfitt, Tom Parker, Alex Strauss, and Claeson Wyckloff.

6.8 References

[1] K. Izzetoglu, S. Bunce, M. Izzetoglu, B. Onaral, and K. Pourrezaei, “Functional Near-Infrared Neuroimaging,” presented at the Proc. IEEE EMBS, 2004.

[2] R. McKendrick, H. Ayaz, R. Olmstead, and R. Parasuraman, “Enhancing Dual-Task Performance with Verbal and Spatial Working Memory Training: Continuous Monitoring of Cerebral Hemodynamics with NIRS.,” *Neuroimage*, 2013.

[3] L. Hirshfield, R. Gulotta, S. Hirshfield, S. Hincks, M. Russell, T. Williams, and R. Jacob, “This is your brain on interfaces: enhancing usability testing with functional near infrared spectroscopy,” presented at the SIGCHI, 2011.

[4] Ferrari M and Q. V., “A brief review on the history of human functional near-infrared spectroscopy (fNIRS) development and fields of application.,” *Neuroimage*, vol. 63, no. 2, pp. 921–35, 2012.

[5] B. Chance, E. Anday, S. Nioka, S. Zhou, L. Hong, K. Worden, C. Li, T. Murray, Y. Ovetsky, and R. Thomas, “A novel method for fast imaging of brain function, non-invasively, with light,” *Optics Express*, vol. 10, no. 2, pp. 411–423, 1988.

[6] B. Chance, E. Anday, S. Nioka, S. Zhou, L. Hong, K. Worden, C. Li, T. Murray, Y. Ovetsky, and R. Thomas, "A novel method for fast imaging of brain function, non-invasively, with light," *Optics Express*, vol. 10, no. 2, pp. 411–423, 1988.

[7] E. Solovey, A. Girouard, K. Chauncey, L. Hirshfield, A. Sassaroli, F. Zheng, S. Fantini, and R. Jacob, "Using fNIRS Brain Sensing in Realistic HCI Settings: Experiments and Guidelines," presented at the ACM UIST Symposium on User Interface Software and Technology, 2009.

[8] A. Devaraj, "Signal Processing for Functional Near Infrared Neuroimaging.," Drexel, 2005.

[9] Q. Zhang, E. Brown, and G. Strangman, "Adaptive filtering for global interference cancellation and real-time recovery of evoked brain activity: a Monte Carlo simulation study," *Journal of biomedical optics*, vol. 12, 2007.

[10] L. M. Hirshfield, "Enhancing Usabiltiy Testing with Functional Near Infrared Spectroscopy," Tufts University, Medford, MA, 2009.

[11] A. Devaraj, M. Izzetoglu, K. Izzetoglu, and B. Onaral, "Motion Artifact Removal for fNIR Spectroscopy for Real World Application Areas," *Proceedings of the SPIE International Society for Optical Engineering*, vol. 5588, pp. 224–229, 2004.

[12] L. M. Hirshfield, P. Bobko, A. Barelka, S. Hirshfield, S. Hincks, S. Gulbrunson, M. Farrington, and D. Paverman, "Using Non-Invasive Brain Measurement to Explore the Psychological Effects of Computer Malfunctions on Users During Human-Computer Interactions," *Advances in Human-Computer Interaction*, 2014.

[13] L. Hirshfield, R. Gulotta, S. Hirshfield, S. Hincks, M. Russell, T. Williams, and R. Jacob, "This is your brain on interfaces: enhancing usability testing with functional near infrared spectroscopy," presented at the SIGCHI, 2011.

[14] L. M. Hirshfield, E. T. Solovey, A. Girouard, J. Kebinger, R. J. K. Jacob, A. Sassaroli, and S. Fantini, "Brain Measurement for Usability Testing and Adaptive Interfaces: An Example of Uncovering Syntactic Workload in the Brain Using Functional Near Infrared Spectroscopy," presented at the Conference on Human Factors in Computing Systems: Proceeding of the twenty-seventh annual SIGCHI conference on Human factors in computing systems, 2009.

[15] J. M. S. Oline V. Olesen, "List-Mode PET Motion Correction Using Markerless Head Tracking: Proof-of-Concept With Scans of Human Subject," *IEEE transactions on medical imaging*, vol. 32, no. 2, 2012.

[16] Q. Cai, A. Sankaranarayanan, Q. Zhang, Z. Zhang, and Z. Liu, "Real Time Head Pose Tracking from Multiple Cameras with a Generic Model," in *IEEE Workshop on Analysis and Modeling of Faces and Gestures in conjunction with CVPR 2010*, 2010.

[17] J. M. Kainerstorfer, P. D. Smith, and A. H. Gandjbakhche, "Noncontact Wide-Field Multispectral Imaging for Tissue Characterization," *IEEE Journal of Selected Topics in Quantum Electronics*, vol. 18, no. 4.

[18] K. T. Sweeney, H. Ayaz, T. E. Ward, M. Izzetoglu, S. F. McLoone, and B. Onaral, "A methodology for validating artifact removal techniques for fNIRS," *Conf Proc IEEE Eng Med Biol Soc*, vol. 2011, pp. 4943–4946, 2011.

6.9 Appendix – Review of Literature on Motion Artifact Correction

This work occurred over the course of several years, and it would not have been possible without support, at various times, from a handful of skilled interdisciplinary

Motion artifact correction

This section provides an overview of motion artifact correction techniques, and it details the techniques that we tested on our datasets. In local fNIRS measurements, the origin of difficult-to-correct noise tends to be motion artifact, which causes a slight decoupling between the sensor and the skin. In a remote sensing context, this issue is magnified, since even the slightest movement (which in the stationary context might not cause sensor-skin decoupling) results in the light taking a somewhat different path through the tissue and back to the sensor, resulting in a new area being probed.

In a local sensing context, several methods have been explored for motion correction beyond basic bandpass filtering. Complementary devices such as an accelerometer or a short-separation fNIRS channel can be used to describe and remove noise. But these may be insufficient for the present context. In this report, we first describe an approach which we think should solve the problem in future experiments, before describing progress applying the more sophisticated fNIRS post-processing techniques.

Motion Correction by Concurrent Image Processing

With the addition of an ordinary camera, you could quantify the amount of motion between measurements. Each pixel of skin can be distinguished from its neighbor in an image. When this difference is amplified, the difference can be visualized.

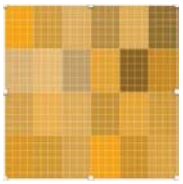

In the current setup, the remote fNIRS always aims at the same location but the target moves. The ordinary camera would have an initial pixel signature for the exact location the fNIRS was measuring.

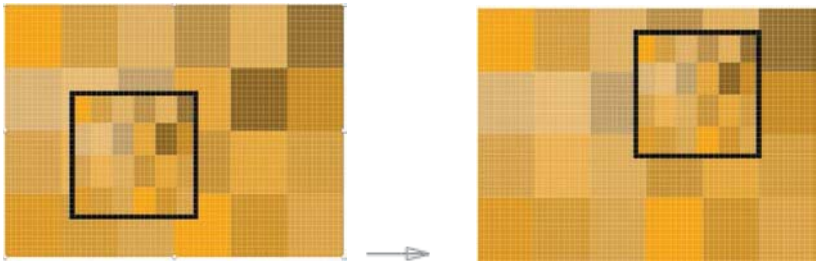

When that pixel group switched location, the associated data could be tagged with a measure quantifying the degree and angle of movement. A team at MIT provides open source Matlab code for this type of video processing and motion amplification. Under controlled conditions, the researchers used this codebase to recover sound from images (Durand, 2015). (Sound is a physical force which causes predictable movements to objects; when that movement is amplified, the sound can be reverse engineered).

The motion-tagging system could then be used to reject measurements or trials, as well as provide quantitative grounds for additional smoothing. In a more advanced setup, the remote

fNIRS could move adaptively in response to how the pixel-set-under-investigation had moved. It could therefore guarantee that it always targeted the same region, minimizing the angle between subject and sensor.

Movable fNIRS

Given that the major affordance of remote sensing (compared to local sensing) is positional flexibility, it makes sense to start iterating on technology for placing the sensor on a digitally controllable stand as quickly as possible.

This would allow for multiple regions to be probed simultaneously with little additional effort. Thinking about the brain as a neatly organized system, with isolated regions, independently computing some specific cognitive function, is becoming outdated in modern neuroscience. The moderate localization of the brain is sufficient to make better-than-chance estimates about cognitive state in a single probe setup. But in a more accurate system for predicting cognitive state, the brain needs to be recognized as a network, where the relevant information is contained in traffic and interneuronal communication - in fNIRS terms, the conditional activation between oxygenation values at different regions.

With a flexible probing setup, in cross-talk with concurrent data processing, probe movement patterns could be calibrated for each subject's brain. A standard cognitive workload procedure might be thought of as a series of binary searches over the user's forehead. In a conservative estimate, fNIRS could probe 10 unique locations a second and only need to revisit a location every 3 seconds (bound by the movement of blood). This means each trial could evaluate 30 different regions. The user would perform an easy and a hard version of the workload induction task, as the fNIRS collected data on those 30 regions. It would then rank these regions by the separability of their time series between the easy and hard trial, as well as the regions between-region similarity, favoring regions which had low correlation in one trial but high in another trial.

With the information obtained from the first pair of trials, subsequent trials could then be used to search the most informative regions with further precision. In one calibration style, there would be three types of region search, and you would continuously change the amount of camera attention dedicated to a particular type. Each pair of trials would complete a mixture of randomly searching for new regions, investigating a broader area near the best region, and collecting more information about the best region. Over multiple trials, the software would gradually discover, with precision beyond that afforded by ordinary fNIRS, the most effective regions for discriminating different classes of cognitive workload on that subject. The most effective regions discovered from one subject would inform the starting point of search for future subjects.

Once calibrated on a satisfactory set of regions, the movability of fNIRS can instead be leveraged for concurrently measuring other subjects. If no other subjects are present, then it can probe a larger surface area around the best regions, and average the different values. This averaging should function as a form of motion correction, since the effect of individual movement is made less drastic.

Adaptive Filtering

An ordinary camera (Poh, 2010) or a slight modification to the remote fNIRS setup may also be used to perform adaptive filtering. Adaptive filtering is a promising technique for filtering systemic trends in local fNIRS data (Zhang, 2009). Bandpass filtering successfully removes breathing and heart rate. But it leaves in tact spontaneous low frequency oscillations that do not have neurological origin. These oscillations would be present in both a shallow and deep source-detector pairing, and could be eliminated from the deep source-detector pairing with knowledge about what frequencies were common between them.

Wavelet filtering

In addition, we have explored the capability of a more extensive motion filtering approach (beyond basic bandpass filtering) on the existing data. We have applied the Wavelet-MDL detrending algorithm proposed in Jang, 2009. In the analysis of local fNIRS data, a noisy global trend, occurring because of breathing or cardiovascular patterns, motion, instrument instability, or other experimental noise, can interfere with the signal.

In previous analyses, we have applied bandpass filtering with cut-offs at 0.01 and 0.1 hz, meaning we expect the signal of interest to oscillate at a scale somewhere between ten and a hundred seconds, and deem any other high frequency or low frequency trends to be noise. But, especially considering the unpredictability of a remote processing setup, noise components could exist at very similar frequency bands to where we expect our signal. Thus, the need for a more advanced filtering technique.

The Wavelet-MDL filter has been found to mitigate noisy trends by decomposing fNIRS measurements into its constituent global trends and noise components, and recharacterizing the signal so that it only contains meaningful hemodynamic trends. We have all of our graphs from the wavelet detrending if you'd like to see them (in the end we chose spline interpolation, which is used in the graphs presented below)

Spline Interpolation

The spline interpolation approach we evaluated is that described by Scholkmann et al. (2010). Once periods of motion artifact have been defined each of those periods is modeled one by one, through-out each fNIRS time-course using the functions pulled from the 'SPM for fNIRS Toolbox'. Each period of modeled data is then subtracted from that period of the original data. In order to produce a continuous signal all the data points after the start of the corrected motion segment are shifted by a constant value. This value is defined as the difference between the mean of the signal at the start of the corrected motion period and the mean of the signal prior to the corrected motion period. The durations over which these means are calculated must be variable, as the length of motion artifacts and the length of the data prior to each motion artifact is also variable. These durations were defined using the framework set out in Scholkmann et al. (2010). This approach was ultimately chosen as the best approach and used on the data presented in this report. In addition to being the best performer in comparisons made of various artifact correction techniques in the literature, this algorithm yielded the best results on our dataset.

7.0 TRUST IN SOFTWARE CODE

The trust in software code project comprised several experimental studies intended to validate elements of the proposed descriptive model of computer code trustworthiness as defined in a cognitive task analysis conducted under ICER Task Order 30 (Alarcon, Militello, Ryan, Jessup, Calhoun, & Lyons, 2016). This research, including the report described below, was instantiated through two separate studies. Study 1 examined readability, organization, and reputation while Study 2 examined commenting style, validity, and placement. Both studies were replicated using "in-person" and virtual (Mechanical Turk) software programmers as participants.

7.1 Introduction

When software code is acquired from a third party or version control repository, programmers assign a level of trust to the code. This trust prompts them to use the code as-is, make minor changes, or rewrite it, which can increase costs and delay deployment. This paper discusses types of degradations to code based on readability and organization expectations and how to present that code as part of a study on programmer trust. Degradations were applied to sixteen of